Progress in Natural Science: Materials International 36 (2026) 143–151

HOSTED BY

Contents lists available at ScienceDirect

Progress in Natural Science: Materials International

journal homepage: www.elsevier.com/locate/pnsmi

Effect of sputtering time and RF power on the properties of CdS thin films prepared by annealing Cd/CdS precursors

Junwei Zhao[a,b], Rengang Zhang[a,*], Tuantuan Wang[a], Peilun Li[a,b], Huihui Zhou[a], Hongyu Liu[a], Peng Zhang[b,**], Runsheng Yu[b], Xingzhong Cao[b]

[a] College of Science, Wuhan University of Science and Technology, Wuhan, 430065, PR China
[b] Institution of High Energy Physics, Chinese Academy of Sciences, Beijing, 100049, PR China

ARTICLE INFO

Keywords:
CdS thin films
Sputtering
Cd/CdS precursors
Annealing
Optical properties

ABSTRACT

CdS thin films were fabricated by annealing precursors which were deposited using the method of Sputtering, Evaporation and Sputtering (SES). Effect of sputtering time and RF power on the structural, compositional, surface morphology and optical properties of CdS thin films was investigated by X-ray diffraction (XRD), scanning electron microscopy (SEM), energy dispersion spectrometer (EDS), UV-Vis spectrophotometer and photoluminescence (PL). The results reveal that the properties and growth of the obtained CdS films are greatly influenced by the second sputtering time rather than the first sputtering time. The deposited precursors are substrate/Cd/CdS, and transformed to CdS after annealing. The CdS films are hexagonal structure with a preferred orientation along (002) plane. Besides, the dense CdS films without cracks or pinholes have S/Cd atomic ratios of 0.87–0.99. Additionally, the grain size, morphology and composition of CdS films change with increasing RF power from 80 W to 150 W. All CdS films have a high average transmittance and band gaps of 2.25–2.43 eV. The PL emission peaks at 530 nm for CdS thin films are possibly caused by the band edge emission while the PL emission peaks at 680 nm arise from sulfur vacancies.

1. Introduction

II-VI semiconductor materials have gained more and more attention due to their numerous optoelectronic applications [1,2]. Cadmium sulfide (CdS) is one of the most popular II-VI semiconductors with a wide direct band gap of 2.47 eV [3], a high refractive index of 2.5, a high transmittance of about 80 %, a high electron mobility of 350 $cm^2V^{-1}s^{-1}$ [4], excellent thermal and chemical stability [5]. CdS has been commonly used for window layers in high efficiency CdTe solar cells, due to the formation of a desirable interfacial layer and lowering the density of interfacial defects [6]. CdTe solar cells, as one of the three most widely commercialized thin film solar cell, have the best power conversion efficiency of 22.1 % [7]. Additionally, CdS has other excellent properties, such as high absorption coefficient and electron affinity [8], high photosensitivity in the range of visible light [9,10], and has been successfully applied to photodetectors [11–14], chemical sensor [15], field-effect transistor [16,17], light-emitting diode (LED) [18], nonlinear optics [19,20], electrochromic devices [21] etc.

During the past decade, the preparation and investigation of CdS thin films and CdS-based devices have received growing interest. Many technologies have been implemented to prepare CdS thin films, such as magnetron sputtering [22,23], molecular beam epitaxy (MBE) [24], thermal evaporation [25], close spaced vapor transport (CSVT) [26], electrodeposition (ED) [27], sol-gel method [28], chemical bath deposition (CBD) [29] and chemical vapor deposition (CVD) [30] etc. Among these technologies, magnetron sputtering is recognized as one of the most attractive methods, which has the advantages of low substrate temperature and large variety of film materials available, higher deposition rate, better adhesion between the film and the substrate. Doroody et al. [29] prepared CdS films by CSVT, CBD and sputtering technology on ultra-thin glass substrates. Their experimental results recommend that the CdS thin films grown by the sputtering might be favourable as the window layer for solar cell application. Latha Marasamy et al. [23] prepared CdS thin films with high average transmittances and thicknesses varying from 40 nm to 100 nm by RF magnetron sputtering to fabricate ultra-thin CdTe solar cells, with their power conversion

* Corresponding author.
** Corresponding author.
E-mail addresses: zhangrengang@wust.edu.cn (R. Zhang), zhangpeng@ihep.ac.cn (P. Zhang).

https://doi.org/10.1016/j.pnsc.2026.01.002
Received 19 September 2025; Received in revised form 30 December 2025; Accepted 3 January 2026
Available online 27 January 2026
1002-0071/© 2026 Chinese Materials Research Society. Published by Elsevier B.V. All rights are reserved, including those for text and data mining, AI training, and similar technologies.

efficiency increased from 1.18 % to 4.13 %. The physical properties of CdS thin films depend on sputtering deposition conditions, such as deposition time [31], sputtering pressure [32], substrate [32,33] and sputtering power [34] etc. It is well known that CdS ceramic targets used for the sputtering have poor thermal conductivity, leading to their cracks during the great-power sputtering process. In contrast, Cd metal targets possess advantages over ceramic ones, such as good thermal and electrical conductivity as well as lower costs. Therefore, investigation of CdS films prepared using Cd metal targets will help to achieve a low-cost preparation process and their potential application in optoelectronic fields.

Recently, our research group have successfully prepared ZnSe films prepared by annealing SES precursors deposited using metal targets [35]. The results indicate that the grain size, composition, morphology and optical properties of the prepared ZnSe films are controlled by sputtering and evaporation parameters, and the precursors for preparing ZnSe films are substrate/Zn/Se/Zn structure. In this work, CdS thin films were fabricated through annealing precursors which were deposited by SES process using Cd target and sulfur powder. The growth mechanism of precursors and CdS thin films is investigated in detail. In addition, the effect of sputtering time and RF power on the properties of the CdS thin films is discussed.

2. Experimental details

2.1. Materials

Cd targets (4N purity, 6 cm diameter, 0.5 cm thickness); sublimed sulfur powder (purity ≥99.5 %); quartz glass substrates (1 mm × 12 mm × 24 mm); a molybdenum boat for evaporation.

2.2. Preparation of CdS thin films

Deposition of precursors was performed in a vacuum chamber equipped with a RF magnetron sputtering system and a resistive evaporation equipment. Before the deposition, the substrates were immersed in deionized water, acetone, and alcohol for ultrasonic cleaning for 15 min, respectively. The background vacuum of chamber was pumped to 4.0×10^{-3} Pa. Then the surface oxides of the Cd target were removed by pre-sputtering for 5 min prior to the formal sputtering process.

The process parameters employed during the preparation of precursors and the preparation diagram of CdS films are shown in Table 1 and Fig. 1, respectively. The SES deposition process of precursors is as follows.

(I) Sputtering: The first step was to deposit Cd onto a substrate surface via RF magnetron sputtering of the Cd target.
(II) Evaporation: The second step was to evaporate sulfur powders under the vacuum condition of 0.1 Pa using a thermal evaporation system.
(III) Sputtering: The third step was to deposit CdS using the same process as step (I).

Finally, the precursors were annealed under an argon atmosphere at 400 °C for 1 h to form CdS thin films. Before heating, the base vacuum of the quartz tube in annealing furnace was pumped to 50 Pa using mechanical pump.

In this work, the CdS thin films obtained with various sputtering times and various RF powers were divided into two groups, respectively.

(I) The first group was performed with t1 (the first sputtering time)/ t2 (the second sputtering time) = 2 min/4 min, 3 min/3 min and 4 min/2 min, then annealed for 1 h under argon atmosphere, which were denoted as C2-4, C3-3, C4-2, respectively.
(II) The second group was performed with t1/t2 = 2 min/4 min and varied RF powers of 80 W, 100 W (namely C2-4), and 150 W, then annealed for 1 h under argon atmosphere, which were denoted as W80, W100, W150, respectively.

In addition, in order to study the formation mechanism of the precursors and CdS films, we prepared the precursors with t1/t2 = 2 min/ 0 min, and 2 min/4 min, denoted as P2-0 (namely the first and second steps in SES process), P2-4, respectively.

Table 1
The process parameters employed during the preparation of precursors.

Process parameter	Value
Background Pressure	4.0×10^{-3} Pa
Substrate temperature	Room temperature
Distance between substrate and target	13 cm
Ar gas flow rate	7.1 sccm
Sputtering pressure	2.8 Pa
The mass of evaporated sulfur	300 mg
Evaporation current	55 A
Distance between substrate and boat	20 cm

2.3. Characterization of thin films

The crystal phase and structure of the thin films were investigated by X-ray diffraction (SmartLab SE) using Cu-Kα radiation (λ = 1.5406 Å). The chemical composition and surface morphology of the thin films were recorded using field emission scanning electron microscopy (FEI NOVA 400 NanoSEM) equipped with an energy dispersion spectrometer (INCAIE350 PentaFETX-3EDS). The transmittance spectra were measured with an ultraviolet–visible (UV-Vis) spectrophotometer (UV-2600) in the wavelength range of 200–900 nm. Photoluminescence measurement was recorded by FL technique (F-7000 FL Spectrophotometer). The thicknesses of the films were measured using probe-type step meter (Alpha-Step D-600).

3. Results and discussion

3.1. Structural analysis

XRD patterns of the precursors and CdS thin films are depicted in Fig. 2. As can be seen in Fig. 2(a), C2-4, C3-3 and C4-2 show only one peak at 2θ = 26.5°, corresponding to the (002) crystal plane of the hexagonal CdS (PDF#77–2306). It is observed that the intensity of the 26.5° peak increases with t2 increased from 2 min to 4 min, indicating higher crystallinity of the CdS thin films. On the contrary, the intensity of the 26.5° peak decreases with increasing t1. Therefore, it is speculated that CdS is produced in the second sputtering process (namely the step (III) of SES), which is conducive to the growth of CdS grains during annealing. And the second sputtering during SES can be the main factor affecting the growth and structure of the annealed CdS films. To validate this hypothesis, we fabricated P2-0 and P2-4 precursors. As shown in Fig. 2(b), a XRD peak at 2θ = 26.5° appears in P2-4 precursor. However, no XRD peak is observed in P2-0 precursor. It confirms that the CdS in P2-4 precursor is formed during the second sputtering process of SES, while S_2 originated from evaporated sulfur during the step (II) of SES. It is considered that the P2-4 precursor formed at room temperature is substrate/Cd/CdS.

The reactive deposition of CdS during the step (III) of SES is as follows:

$$\mathrm{Cd\ (g)} + \frac{1}{2}\mathrm{S_2\ (g)} \rightarrow \mathrm{CdS(s)} \tag{3-1}$$

The reaction was analyzed using the thermochemical arguments, and equations (3)–(2) was used to calculate the standard Gibbs free-energy changes ($\Delta_r G_T^0$) [36]

$$\Delta_r G_T^0 = \sum\nolimits_{\mathrm{B}} \nu_B \Delta_{\mathrm{f}} \mathrm{G}_{\mathrm{T,B}}^0 \tag{3-2}$$

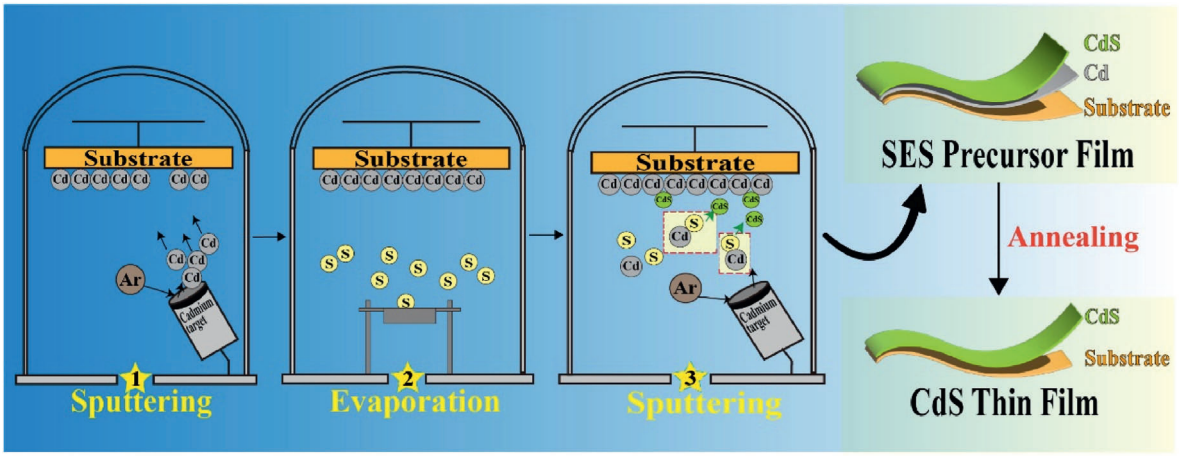

Fig. 1. Schematic diagram of the CdS film preparation process.

As a result, the $\Delta_r G_T^0$ value for the reaction at room temperature is estimated to be −183.562 kJ/mol. Based on $\Delta_r G_T^0 < 0$, it is believed that the reaction is the spontaneous process to the right at room temperature, thermodynamically confirming that the step (III) of SES is a reactive sputtering deposition of CdS. The formation process of CdS films is believed to be as follows:

(1) Cd is deposited on substrate surface during the step (I) of SES.
(2) S_2 is generated during the step (II) of SES.
(3) CdS is formed by the reaction (3-1) and deposited on the substrate/Cd surface during the step (III) of SES.
(4) The deposited substrate/Cd/CdS (precursor) is converted to substrate/CdS during annealing, accompanied by crystal growth.

CdS formation process is different from the previous report about ZnSe [35]. This can be explained by the different physical and chemical properties for sulfur and selenium. S has a melting point of 115 °C and a boiling point of 445 °C, while Se has a melting point of 221 °C and a boiling point of 685 °C, indicating the easy volatilization of sulfur. So reactive sputtering deposition of CdS rather than ZnSe during the step (III) of SES can occur.

The XRD patterns of W80, W100 and W150 are depicted in Fig. 2(c). A prominent CdS (002) peak at $2\theta = 26.5°$ is observed for the CdS thin films. The intensity of the (002) diffraction peak becomes greater as the RF power is raised from 80 W to 150 W, indicating the increased crystallinity. The reason is that with the increase of RF power, the deposition rate increases accordingly, therefore the number of sputtered atoms per unit time is more, resulting in more Cd/CdS deposited on the substrate surface, which is conducive to the crystallization and growth of the CdS thin films during annealing precursors. As seen from XRD patterns, it is found that the intensity of the 26.5° peak for all CdS films is considerably stronger than the other peaks, indicating that the CdS films grow along the preferential orientation of the (002) plane of hexagonal CdS due to its lowest surface free energy [9,37,38]. The strong peak of CdS films prepared by RF magnetron sputtering of the ceramic target was also observed by Kim et al. [39].

Furthermore, structural parameters were calculated for CdS thin films as shown in Table 2. The interplanar spacing (D_{hkl}) of the prominent (002) plane was estimated using Debye-Scherrer formula [40].

$$D_{hkl} = \frac{0.9\lambda}{\beta \cos\theta} \tag{3-3}$$

Here, λ is the incident X-ray wavelength (λ = 1.5406 Å, Kα (Cu)). β is the full width at half maximum (FWHM), and θ is Bragg angle at (hkl) plane.

The microscopic strain (ε) of the annealed CdS thin films was calculated by the relation [41].

$$\varepsilon = \frac{\beta \cot\theta}{4} \tag{3-4}$$

The dislocation density (δ) was calculated by the relation [42].

$$\delta = \frac{n}{D^2} \tag{3-5}$$

Here, D is the average crystallite size. n is the factor, and the dislocation density is minimized when the factor is equal to 1.

As shown in Table 2, the calculated crystallite size of C2-4 is 41 nm, which is the largest in the first group, implying the best crystallinity for CdS thin film. In the case of constant total time, with increasing t2 from 2 min to 4 min, more CdS are deposited in the second sputtering process, resulting in the increased grain size of CdS thin films during annealing. In the annealing process of the SES precursors, annealing temperature is higher than the melting point of Cd, and the kinetic energies of the inner atoms of the precursors are higher, which facilitates outward diffusion and aggregation of Cd and CdS in the precursors, promoting the growth of CdS grains. Thus, we conclude that both the inner Cd and outer CdS are beneficial to CdS grain growth during annealing, but the outer CdS plays a major role in the CdS grain growth. Besides, as shown in Table 2, the d values of CdS thin films are less than the standard value of 0.3563 nm (PDF#77–2306), indicating that vacancies occur in the films. As seen from Table 2, with the increase of RF power, due to increased Cd and CdS deposition, the crystallite size of the annealed CdS thin films increases. Accordingly the microscopic strain and dislocation density gradually decrease because of the increased crystallinity of the films. It indicates that the CdS thin films prepared by annealing SES precursors have good crystallinity and low dislocation density.

3.2. Compositional analysis

In order to further study the growth mechanism of precursors and CdS thin films, their chemical compositions were studied by EDS. Fig. 3 (a) and (b) show the EDS spectra for P2-0 and P2-4, respectively. As can be seen from Fig. 3(a), Si and O elements are attributed to the quartz glass substrate. The presence of Cd element is found in P2-0, while no S element is observed. For P2-4, Cd and S elements are observed. The presence of S element in P2-4 is believed to originate from reactive sputtering deposition of CdS during the step (III) of SES, which further confirms the XRD analysis. The formation of P2-4 includes: (1) sputtering deposition of Cd in Ar, (2) reactive sputtering deposition of CdS in Ar and S_2 which derived from evaporated sulfur powder during the step (II) of SES. It is also observed in Fig. 3(b, c) that the S/Cd atomic ratio of C2-4 increased compared to P2-4, which is related to the volatilization

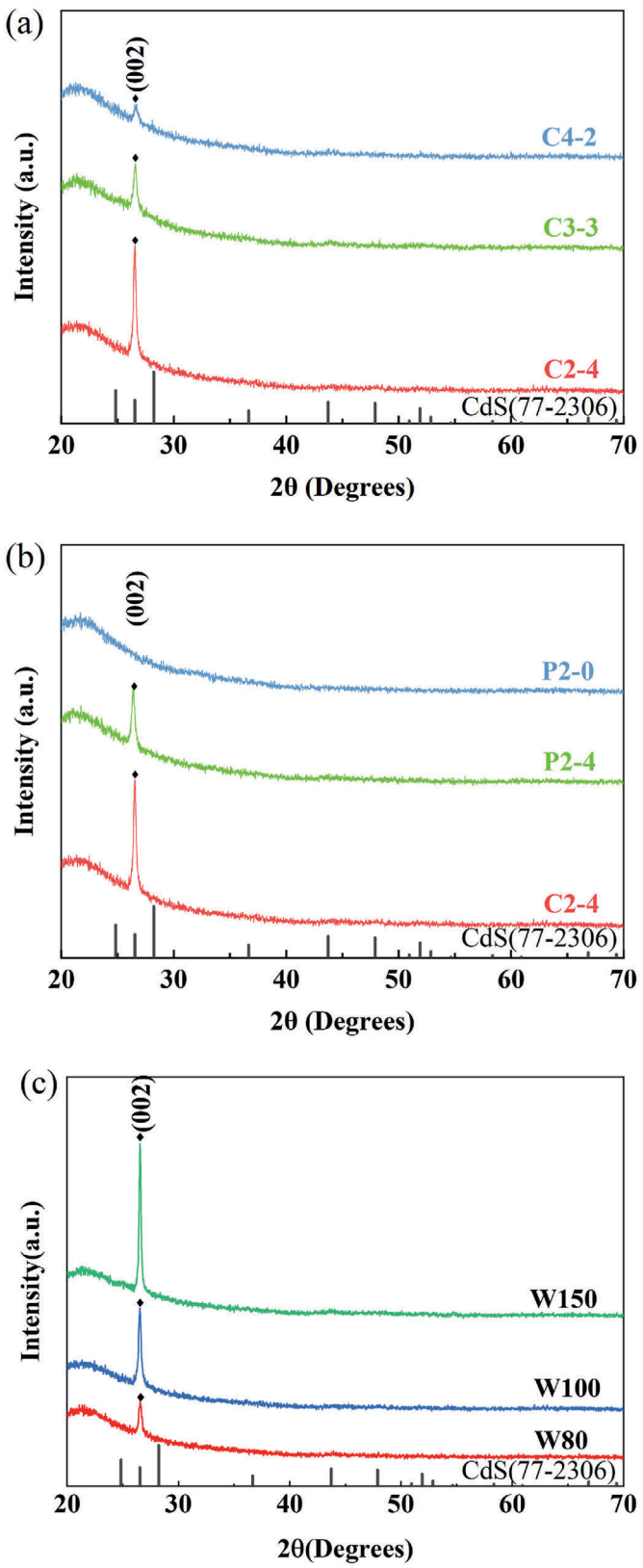

Fig. 2. XRD patterns of (a) CdS films obtained with various sputtering times, (b) the precursors before and after annealing, (c) CdS films obtained with various sputtering powers.

of Cd during annealing precursor. As seen in Fig. 3(c), with the total time fixed at 6min, the S/Cd atomic ratio of CdS thin films increases from 0.87 to 0.99 with the prolonged t2, indicating that the increase of outer CdS in the precursors is more advantageous to obtain better composition and crystallinity of CdS thin films. Fig. 3(d) shows the S/Cd atomic ratio of the CdS thin films obtained with various RF powers. As can be seen, the S/Cd atomic ratio of CdS thin films is in the range of 0.96–0.99. The EDS results show that the composition of these CdS thin films is close to the ideal stoichiometric ratio. The atomic ratio of S/Cd in the W100 reaches the maximum value of approximately 0.99. The EDS analyses are well consistent with the XRD and SEM results, showing that the growth of CdS thin films during annealing is accompanied by the Cd volatilization and their good compositions can be obtained by annealing SES precursors.

3.3. Morphological analysis

SEM images of the CdS thin films obtained with different sputtering times are presented in Fig. 4(a–c). The obtained CdS thin film is dense, with no micro-cracks or pinholes. As t2 decreases from 4 min to 3 min, some great aggregations appear on the surface of the CdS thin film. When t2 decreases to 2 min, aggregations on the surface of C4-2 are almost observed. SEM images of CdS thin films obtained with different RF powers are presented in Fig. 4(d–f). With the increase of RF power, the grain size of CdS thin films becomes larger and great aggregations appear, which is related to the increase of CdS film thickness [43]. It indicates that the high RF power leads to greater mass of Cd and CdS deposited in the first and second sputtering process, respectively. These are in agreement with the XRD results.

3.4. Optical properties

The transmittance spectra of CdS thin films obtained with different sputtering times are presented in Fig. 5(a). It is clearly observed that compared to P2-4 precursor, C2-4 exhibits higher transmittance in the visible light range and a steep absorption edge near 510 nm, which corresponds with the characteristic absorption of CdS. It indicates that annealing promotes the conversion of Cd/CdS precursor to CdS and improves the uniformity of CdS thin film, further supporting the XRD results. As observed in Fig. 5(a), the annealed CdS thin films have high transmittance of about 80 %. As the t2 decreased to 2 min, the light transmittance of CdS thin film decreases and the characteristic absorption edge is not steep. Combined with the transmittance, composition and crystallinity of the CdS thin films, it is further confirmed that t2 rather than t1 is the main factor affecting the grain growth and properties of CdS thin films. As seen in Fig. 5(b), the light transmittance of W80 remains about 60 % due to the poor crystallinity. When the RF power increases to 100 W, W100 exhibits a steep absorption edge and good light transmittance, indicating good uniformity and high quality of the CdS thin film. When the RF power further increases from 100 W to 150 W, the average light transmittance of CdS thin film has little changes, and the steepness of the absorption edge decreases, possibly due to the increased film thickness. It is found that among these CdS films, C2-4 exhibits the best optical performance and film quality.

The variation of $(\alpha h\nu)^2$ with photon energy $h\nu$ is shown in Fig. 6 for the annealed CdS thin films prepared with different sputtering times and different RF powers. The optical band gaps of CdS films are obtained by extrapolating the linear region of the absorption curves to $h\nu = 0$. As seen in Fig. 6(a), the band gaps of C2-4, C3-3 and C4-2 are 2.36 eV, 2.38 eV and 2.43 eV, respectively. As seen in Fig. 6(b), the band gaps of W80, W100 and W150 are 2.25 eV, 2.36 eV and 2.38 eV, respectively. The CdS thin films prepared by annealing SES precursors have the band-gap values which are close to those of CdS thin films prepared by RF sputtering ceramic targets [44].

Room-temperature PL spectra for the CdS films are presented in Fig. 7. The strong PL emission peak at about 530 nm could be attributed to the band-edge transition of CdS, which is due to radiative recombination involving impurity levels near the band edge [45,46]. It is notable that in Fig. 7(a), the strongest 530 nm emission peak is observed for

Table 2
Structural parameters of CdS films obtained by annealing precursors.

sample	Crystalline plane	FWHM (deg.)	Crystallite size (nm)	D_{hkl} (nm)	ε ($\times 10^{-3}$)	δ ($\times 10^{12}$)(cm^{-2})
C2-4	(002)	0.199	41	0.3356	3.68	0.06
C3-3	(002)	0.215	38	0.3347	3.97	0.07
C4-2	(002)	0.399	21	0.3343	7.35	0.24
W80	(002)	0.220	37	0.3352	4.07	0.07
W100	(002)	0.199	41	0.3356	3.68	0.06
W150	(002)	0.158	52	0.3357	2.93	0.04

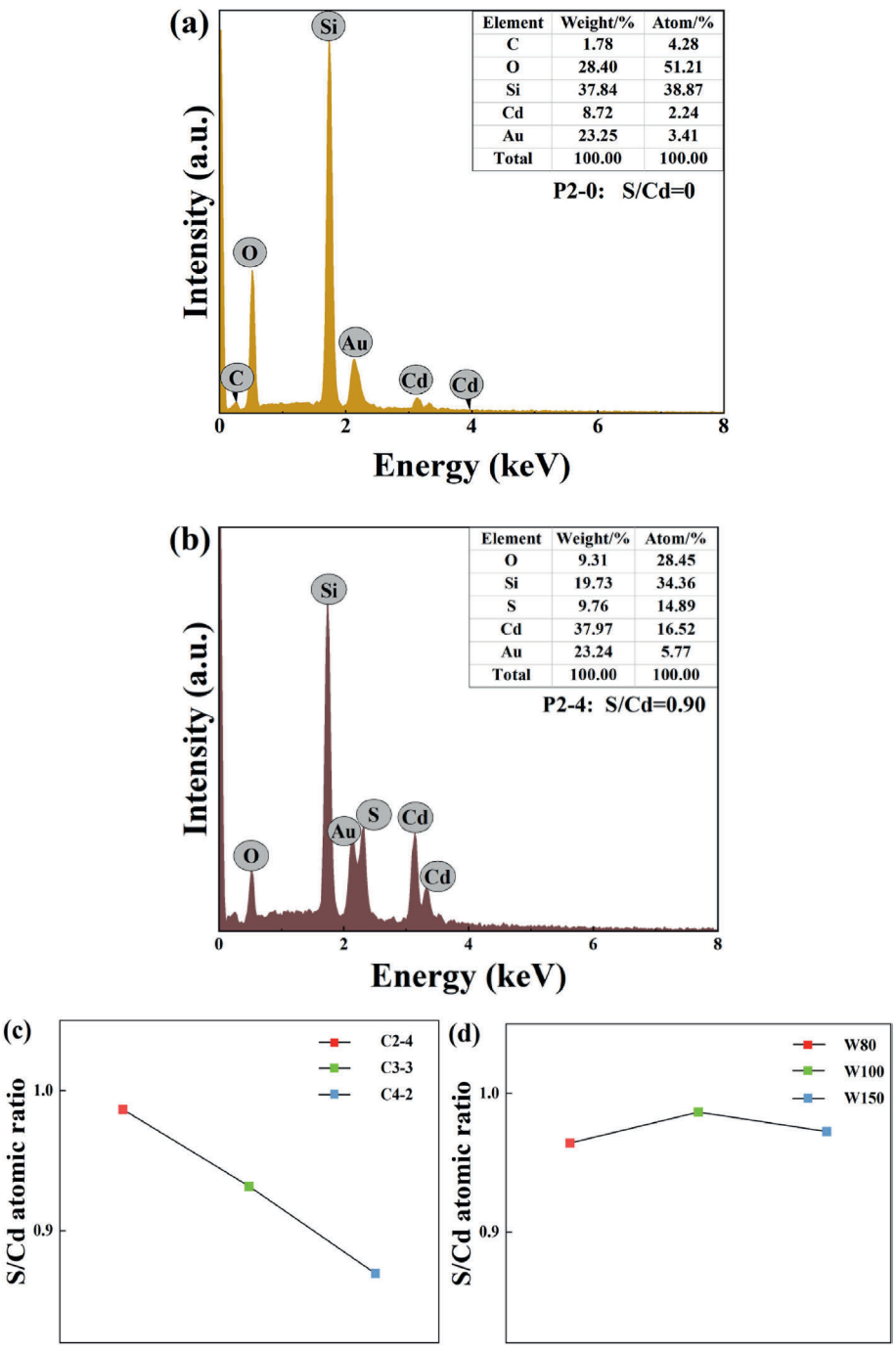

Fig. 3. EDS spectra of (a) P2-0, (b) P2-4 precursors and composition of CdS thin films prepared by annealing of SES precursors deposited for (c) various sputtering times and (d) various RF powers.

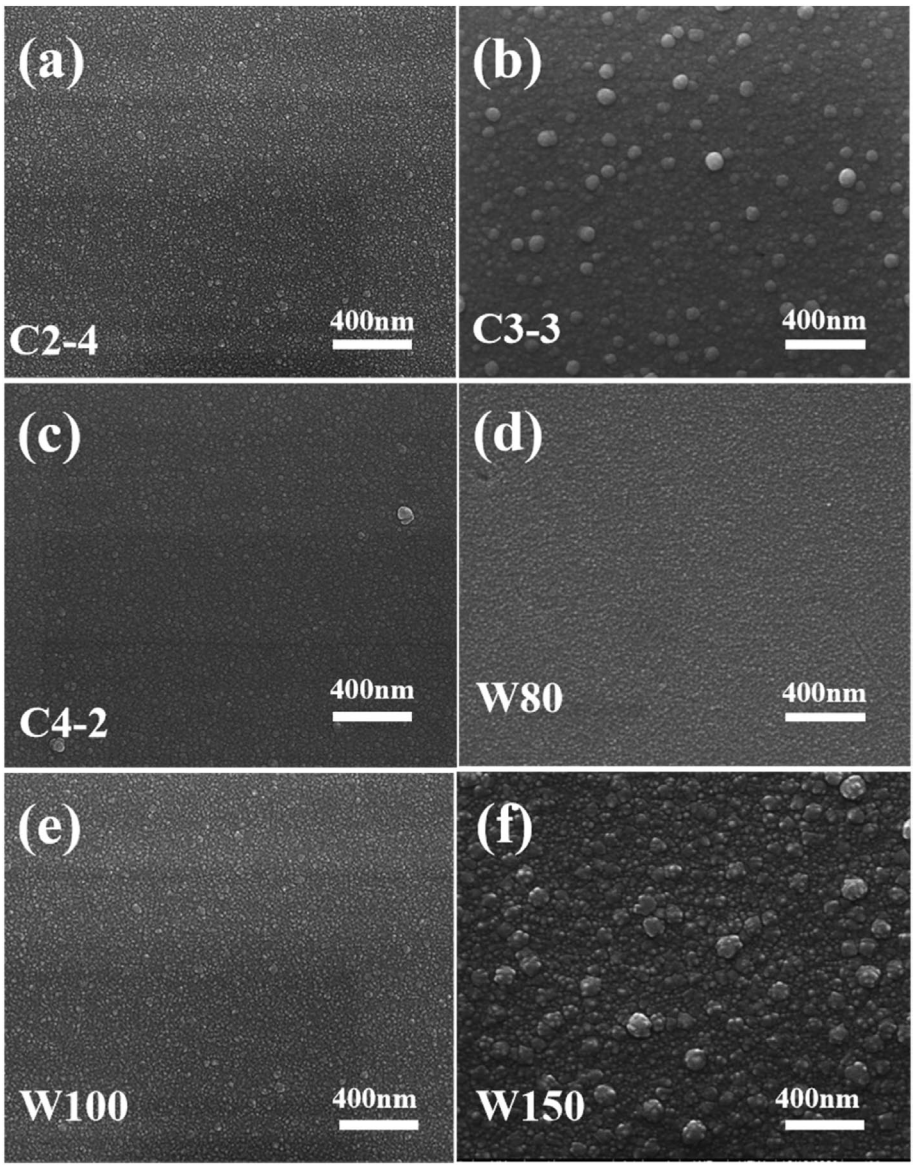

Fig. 4. SEM morphology of the CdS thin films obtained with (a–c) various sputtering times and (d–f) various sputtering powers.

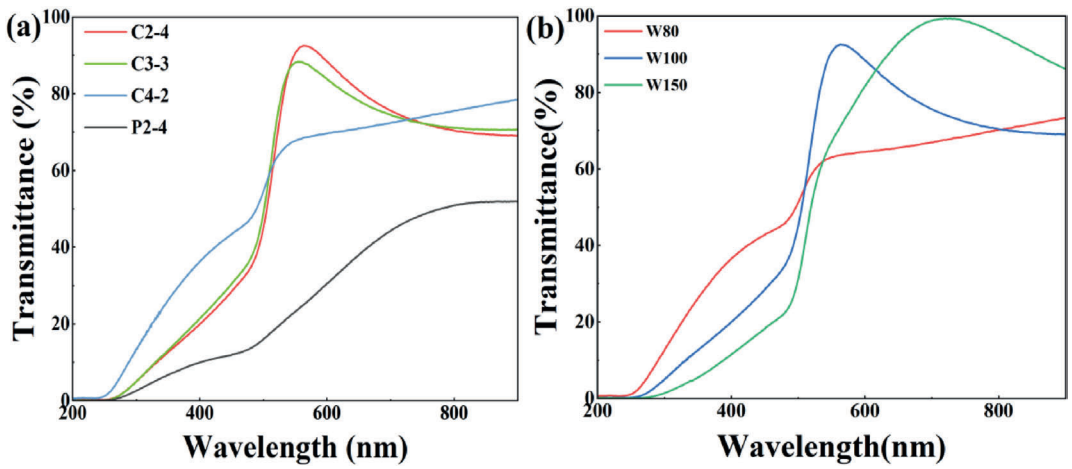

Fig. 5. The UV–Vis transmission spectra of (a) P2-4 precursor and CdS thin films obtained with different sputtering times, (b) CdS thin films obtained with different RF powers.

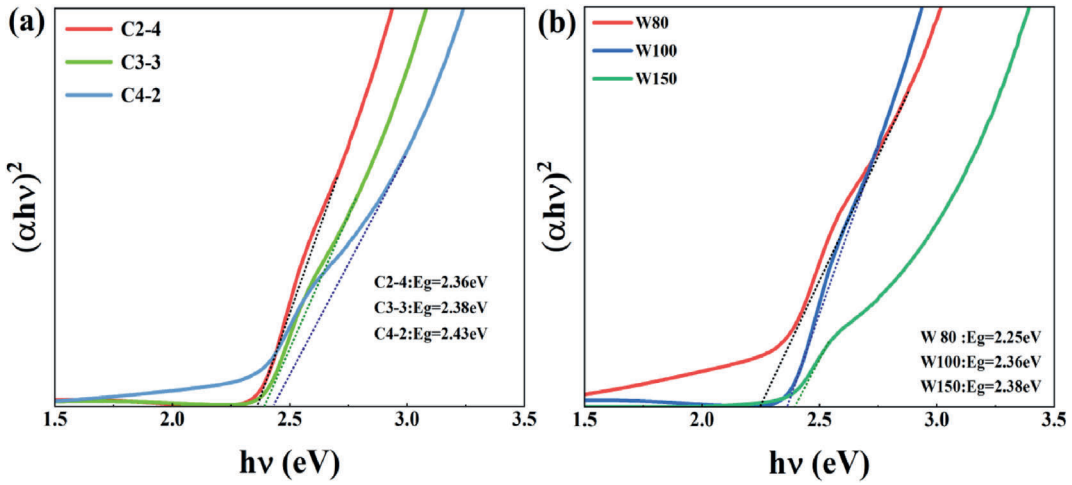

Fig. 6. The variation of $(\alpha h\nu)^2$ with photon energy hν for CdS thin films prepared with (a) different sputtering times and (b) different RF powers.

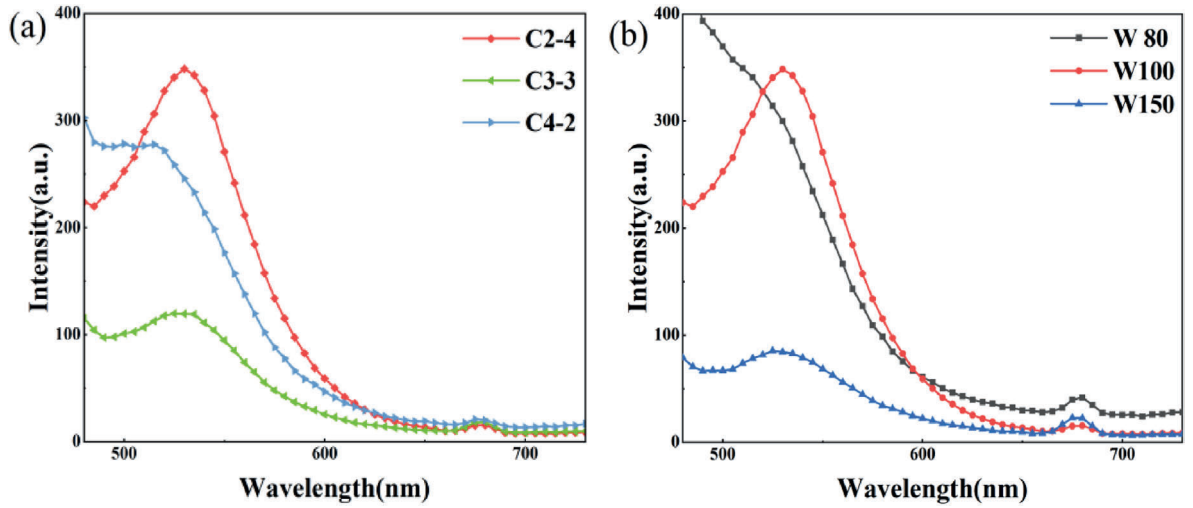

Fig. 7. PL spectra of CdS thin films obtained with (a) different sputtering times and (b) different sputtering powers.

C2-4, indicating its strong band edge emission and good crystal quality. The 530 nm emission peak of the C4-2 is weak, due to its poor crystallinity caused by the smallest deposition time of the CdS in the precursor. Also, the weak peaks at about 680 nm are observed in Fig. 7(a) for all CdS films, possibly arising from sulfur vacancies [47]. The weak 680 nm emission peaks indicate their low defect concentrations. As seen in Fig. 7 (b), the PL emission peak of W80 at 530 nm is very weak, which is similar to the results of C4-2. This is due to its poor crystallinity of the CdS thin film and an increased defect concentration caused by low RF power and low deposition rate being not conducive to the formation and growth of CdS grains. When the RF power increases to 100 W and 150 W, the intensity of the 530 nm emission peak increases, indicating decreased sulfur vacancies and improved film quality. Therefore it is believed that increasing the t2 and RF power can effectively enhance the quality of CdS thin films prepared by annealing SES precursors.

4. Conclusion

We successfully fabricated high-quality CdS thin films by annealing SES precursors. The results show that the precursors are substrate/Cd/CdS, which are transformed to CdS after annealing. All CdS films without cracks or pinholes exhibit a hexagonal structure with a preferred orientation along the (002) plane. The second sputter-deposition during SES is the main influencing factor of the growth and properties of CdS films. With increasing t2, the crystallite size of CdS films increases from 21 nm to 41 nm, and the S/Cd atomic ratio increases from 0.87 to 0.99, confirming that the increased t2 promotes CdS crystallization during annealing. The annealed CdS films have high transmittance of about 80 % and band gap values of 2.36–2.43 eV. Besides, with increasing the RF power, the crystallinity of CdS films increases, while grain agglomerations occur. Moreover, these CdS films show the 530 nm emission peaks attributed to the band-edge emission, but the peaks of C4-2 and W80 are obviously weak due to their poor crystallinity. For all CdS films, the weak emission peaks at about 680 nm are probably derived from sulfur vacancies, indicating their low defect concentration. Additionally, further optimization and investigation of CdS thin films prepared using metal targets and annealing-free process are crucial for improving film quality, their fundamentals and application, which will be implemented in the next stage of our research.

CRediT authorship contribution statement

Junwei Zhao: Writing – original draft, Validation, Methodology, Investigation, Formal analysis, Data curation. **Rengang Zhang:** Writing – review & editing, Supervision, Resources, Methodology, Conceptualization. **Tuantuan Wang:** Writing – review & editing, Methodology, Data curation. **Peilun Li:** Methodology, Investigation, Data curation. **Huihui Zhou:** Investigation, Data curation. **Hongyu Liu:** Validation,

Methodology. **Peng Zhang:** Resources, Conceptualization. **Runsheng Yu:** Supervision. **Xingzhong Cao:** Supervision, Resources.

Funding

This work was supported by the National Natural Science Foundation of China [Grant No.11975173].

Declaration of competing interest

The authors declare that they have no known competing financial interests or personal relationships that could have appeared to influence the work reported in this paper.

References

[1] T. Gupta, R.P. Chauhan, Photocatalytic degradation of water pollutants using II-VI semiconducting catalysts: a comprehensive review, J. Environ. Chem. Eng. 9 (2021) 106734, https://doi.org/10.1016/j.jece.2021.106734.
[2] O.K. Wu, R.D. Rajavel, J.E. Jensen, Status of II–VI molecular-beam epitaxy technology, Mater. Chem. Phys. 43 (1996) 103–107, https://doi.org/10.1016/0254-0584(95)01614-Z.
[3] A. Isha, A. Kowsar, A. Kuddus, M.K. Hossain, M.H. Ali, M.D. Haque, M.F. Rahman, High efficiency Cu2MnSnS4 thin film solar cells with SnS BSF and CdS ETL layers: a numerical simulation, Heliyon 9 (2023) e15716, https://doi.org/10.1016/j.heliyon.2023.e15716.
[4] N.C. Morgante-Guandalini, I.V. Perez-Quintana, L.G. Daza, M. Acosta, J. Méndez-Gamboa, B.C. Muñoz, R. Castro-Rodríguez, Vertical nanostructures thin films of CdS and CdTe using low temperatures GLAD, Physica B 666 (2023) 415075, https://doi.org/10.1016/j.physb.2023.415075.
[5] Y. Dai, X. Wang, W. Peng, C. Xu, C. Wu, K. Dong, R. Liu, Z.L. Wang, Self-powered Si/CdS flexible photodetector with broadband response from 325 to 1550 nm based on pyro-phototronic effect: an approach for photosensing below bandgap energy, Adv. Mater. 30 (2018) 1705893, https://doi.org/10.1002/adma.201705893.
[6] D.R. Sajitha, The emergence of chalcogenides: a new era for thin film solar absorbers, Prog. Solid State Chem. 76 (2024) 100490, https://doi.org/10.1016/j.progsolidstchem.2024.100490.
[7] M. Afzaal, P. O'Brien, Recent developments in II–VI and III–VI semiconductors and their applications in solar cells, J. Mater. Chem. 16 (2006) 1597–1602, https://doi.org/10.1039/B512182E.
[8] S. Yılmaz, S.B. Töreli, İ. Polat, M.A. Olgar, M. Tomakin, E. Bacaksız, Enhancement in the optical and electrical properties of CdS thin films through Ga and K co-doping, Mater. Sci. Semicond. Process. 60 (2017) 45–52, https://doi.org/10.1016/j.mssp.2016.12.016.
[9] A.B.G. Trabelsi, K.V. Chandekar, FatemahH. Alkallas, I.M. Ashraf, J. Hakami, Mohd Shkir, A. Kaushik, S. AlFaify, A comprehensive study on Co-doped CdS nanostructured films fit for optoelectronic applications, J. Mater. Res. Technol. 21 (2022) 3982–4001, https://doi.org/10.1016/j.jmrt.2022.11.002.
[10] D.P. Amalnerkar, Photoconducting and allied properties of CdS thick films, Mater. Chem. Phys. 60 (1999) 1–21, https://doi.org/10.1016/S0254-0584(99)00061-9.
[11] Y. Zhao, Size controllable preparation of sphere-based monolayer CdS thin films for white-light photodetectors, Ceram. Int. 44 (2018) 2407–2412, https://doi.org/10.1016/j.ceramint.2017.10.210.
[12] S. Luo, Y. Yu, N. Cheng, X. Qi, S. Luo, Y. Liu, J. Zhong, Solution-processed GeSe/CdS heterogenous film for self-powered photodetectors, Ceram. Int. 49 (2023) 11302–11310, https://doi.org/10.1016/j.ceramint.2022.11.330.
[13] S. Nagappa Moger, P. Kumar, G.K. Rao, M. M g, Annealing assisted enhancement in photo response of PV deposited CdS thin films, Opt. Laser Technol. 149 (2022) 107868, https://doi.org/10.1016/j.optlastec.2022.107868.
[14] A. Kathalingam, S. Valanarasu, T. Ahamad, S.M. Alshehri, H.-S. Kim, Spray pressure variation effect on the properties of CdS thin films for photodetector applications, Ceram. Int. 47 (2021) 7608–7616, https://doi.org/10.1016/j.ceramint.2020.11.100.
[15] K. Hari Prasad, S. Vinoth, V. Ganesh, R. Ade, Fabrication of Al and La co-doped CdS thin film for ammonia gas-sensing application through low-cost nebulizer spray pyrolysis technique, Appl. Phys. A 130 (2024) 204, https://doi.org/10.1007/s00339-024-07355-4.
[16] L. Li, H. Lu, Z. Yang, L. Tong, Y. Bando, D. Golberg, Bandgap-graded CdS_xSe_{1-x} nanowires for high-performance field-effect transistors and solar cells, Adv. Mater. 25 (2012) 1109–1113, https://doi.org/10.1002/adma.201204434.
[17] B. Mereu, G. Sarau, E. Pentia, V. Draghici, M. Lisca, T. Botila, L. Pintilie, Field-effect transistor based on nanometric thin CdS films, Mater. Sci. Eng. B 109 (2004) 260–263, https://doi.org/10.1016/j.mseb.2003.10.077.
[18] Y.J. Ma, P.F. Ji, Y. Li, Y.L. Song, F.Q. Zhou, A prototypical near-infrared light-emitting diode from CdS/Si heterojunctions based on the defect emissions in the interface, J. Lumin. 240 (2021) 118434, https://doi.org/10.1016/j.jlumin.2021.118434.
[19] B. Suresh, S. Ramachandran, G. Shanmugam, Effect of cerium dopant on third-order nonlinear optical properties of CdS/PEG self-standing nanocomposite films, Opt. Mater. 135 (2023) 113299, https://doi.org/10.1016/j.optmat.2022.113299.
[20] Z.R. Khan, Munirah, Mohd Shkir, A.S. Alshammari, V. Ganesh, S. AlFaify, M. Gandouzi, Structural, linear and third order nonlinear optical properties of sol-gel grown Ag-CdS nanocrystalline thin films, J. Electron. Mater. 48 (2019) 1122–1132, https://doi.org/10.1007/s11664-018-6832-2.
[21] B. Zhang, H. Wang, Y. Xiang, H. Jiang, L. Tang, J. Luo, Y. Tian, Quantum dots CdS-modified WO3 film for multi-color electrochromism, Electrochim. Acta 440 (2023) 141749, https://doi.org/10.1016/j.electacta.2022.141749.
[22] N. Akcay, E.P. Zaretskaya, S. Ozcelik, Development of a CZTS solar cell with CdS buffer layer deposited by RF magnetron sputtering, J. Alloys Compd. 772 (2019) 782–792, https://doi.org/10.1016/j.jallcom.2018.09.126.
[23] L. Marasamy, R. Aruna-Devi, O. Iván Domínguez Robledo, J. Álvaro Chávez Carvayar, N. Enrique Vázquez Barragán, J. Santos-Cruz, S. Andrea Mayén-Hernández, G. Contreras-Puente, M. De La Luz Olvera, F. De Moure Flores, Probing the significance of RF magnetron sputtering conditions on the physical properties of CdS thin films for ultra-thin CdTe photovoltaic applications, Appl. Surf. Sci. 574 (2022) 151640, https://doi.org/10.1016/j.apsusc.2021.151640.
[24] P. Boieriu, R. Sporken, A. Adriaens, Y. Xin, N.D. Browning, S. Sivananthan, SIMS and XPS characterization of CdS/CdTe heterostructures grown by MBE, Nucl. Instrum. Methods Phys. Res., Sect. B 161–163 (2000) 975–979, https://doi.org/10.1016/S0168-583X(99)00926-X.
[25] S. Dolai, R. Dey, S. Hussain, R. Bhar, A. Kumar Pal, Photovoltaic properties of F: SnO2/CdS/CuO/Ag heterojunction solar cell, Mater. Res. Bull. 109 (2019) 1–9, https://doi.org/10.1016/j.materresbull.2018.09.022.
[26] H. Liu, Y. Zhou, Q. Xie, G. Wang, M. Jiang, J. Pan, R. Wang, Suppression of pinhole defects in thin film CdS/CdTe solar cell via gelatin-based negative photoresist passivation, Mater. Sci. Semicond. Process. 148 (2022) 106817, https://doi.org/10.1016/j.mssp.2022.106817.
[27] J. Han, Y. Jian, Y. He, Y. Liu, X. Xiong, L. Cha, V. Krishnakumar, H.-J. Schimper, Nanostructures of CdS thin films prepared by various technologies for thin film solar cells, Mater. Lett. 177 (2016) 5–8, https://doi.org/10.1016/j.matlet.2016.04.111.
[28] R.K. Sonker, B.C. Yadav, V. Gupta, M. Tomar, Synthesis of CdS nanoparticle by sol-gel method as low temperature NO2 sensor, Mater. Chem. Phys. 239 (2020) 121975, https://doi.org/10.1016/j.matchemphys.2019.121975.
[29] C. Doroody, K.S. Rahman, H.N. Rosly, M.N. Harif, M. Isah, Y.B. Kar, S.K. Tiong, N. Amin, A comparative study of CdS thin films grown on ultra-thin glass substrates by RF magnetron sputtering and chemical bath deposition, Mater. Sci. Semicond. Process. 133 (2021) 105935, https://doi.org/10.1016/j.mssp.2021.105935.
[30] M. Arshad Kamran, T. Alharbi, Effect of Al doping on photoluminescence and conductivity of 1D CdS nanobelts synthesized by CVD for optoelectronic applications, J. Sci. Adv. Mater. Devices 7 (2022) 100464, https://doi.org/10.1016/j.jsamd.2022.100464.
[31] X. Hu, J. Tao, Y. Wang, J. Xue, G. Weng, C. Zhang, S. Chen, Z. Zhu, J. Chu, 5.91%-efficient Sb2Se3 solar cells with a radio-frequency magnetron-sputtered CdS buffer layer, Appl. Mater. Today 16 (2019) 367–374, https://doi.org/10.1016/j.apmt.2019.06.001.
[32] Y. Park, E.K. Kim, S. Lee, J. Lee, Growth and characterization of CdS thin films on polymer substrates for photovoltaic applications, J. Nanosci. Nanotechnol. 14 (2014) 3880–3883, https://doi.org/10.1166/jnn.2014.8132.
[33] M.A. Islam, M.S. Hossain, M.M. Aliyu, P. Chelvanathan, Q. Huda, M.R. Karim, K. Sopian, N. Amin, Comparison of structural and optical properties of CdS thin films grown by CSVT, CBD and sputtering techniques, Energy Proc. 33 (2013) 203–213, https://doi.org/10.1016/j.egypro.2013.05.059.
[34] H. Guo, K. Zhang, X. Jia, C. Ma, N. Yuan, J. Ding, Effect of ITO film deposition conditions on ITO and CdS films of semiconductor solar cells, Optik 140 (2017) 322–330, https://doi.org/10.1016/j.ijleo.2017.04.068.
[35] R. Cui, R. Zhang, S. Li, B. Yue, Y. Zhang, H. Liu, P. Zhang, X. Cao, R. Yu, B. Wang, Influence of sputtering time and evaporation current on the properties of ZnSe thin films prepared by annealing SES precursors, Surf. Interfaces 63 (2025), https://doi.org/10.1016/j.surfin.2025.106337, 2468-0230.
[36] R. Zhang, B. Wang, L. Wei, X. Li, Q. Xu, S. Peng, I. Kurash, H. Qian, Growth and properties of ZnS thin films by sulfidation of sputter deposited Zn, Vacuum 86 (2012) 1210–1214, https://doi.org/10.1016/j.vacuum.2011.11.003.
[37] J. Lee, Raman scattering and photoluminescence analysis of B-doped CdS thin films, Thin Solid Films 451–452 (2004) 170–174, https://doi.org/10.1016/j.tsf.2003.10.103.
[38] J.C. Orlianges, C. Champeaux, P. Dutheil, A. Catherinot, T.M. Mejean, Structural, electrical and optical properties of carbon-doped CdS thin films prepared by pulsed-laser deposition, Thin Solid Films 519 (2011) 7611–7614, https://doi.org/10.1016/j.tsf.2010.12.139.
[39] D. Kim, Y. Park, M. Kim, Y. Choi, Y.S. Park, J. Lee, Optical and structural properties of sputtered CdS films for thin film solar cell applications, Mater. Res. Bull. 69 (2015) 78–83, https://doi.org/10.1016/j.materresbull.2015.03.024.
[40] W. Mahmood, J. Ali, I. Zahid, A. Thomas, A. Ul Haq, Optical and electrical studies of CdS thin films with thickness variation, Optik 158 (2018) 1558–1566, https://doi.org/10.1016/j.ijleo.2018.01.045.
[41] S. Sen, K. Halder S, P. Sen, S. Gupta, An X-ray line broadening analysis in the vacuum-evaporated silver films, J. Phys. Soc. Jpn. 38 (1975) 1641–1647, https://doi.org/10.1143/JPSJ.38.1641.
[42] H.N. Rosly, K.S. Rahman, M.N. Harif, et al., Annealing temperature assisted microstructural and optoelectrical properties of CdSe thin film grown by RF magnetron sputtering, Superlattice. Microst. 148 (2020) 106716, https://doi.org/10.1016/j.spmi.2020.106716.
[43] Z. Ghorannevis, E. Akbarnejad, M. Ghoranneviss, Effects of various deposition times and RF powers on CdTe thin film growth using magnetron sputtering,

J Theor Appl Phys 10 (2016) 225–231, https://doi.org/10.1007/s40094-016-0219-7.
[44] S. Chen, R. Yu, L. Song, R. Zhang, X. Cao, B. Wang, P. Zhang, Effect of low temperature vulcanization time on the structure and optical properties of ZnS thin films, Appl. Surf. Sci. 498 (2019) 143876, https://doi.org/10.1016/j.apsusc.2019.143876.
[45] X.L. Tong, D.S. Jiang, Y. Li, Z.M. Liu, M.Z. Luo, The influence of the silicon substrate temperature on structural and optical properties of thin-film cadmium sulfide formed with femtosecond laser deposition, Physica B 382 (2006) 105–109, https://doi.org/10.1016/j.physb.2006.02.012.
[46] M. Karimi, M. Rabiee, F. Moztarzadeh, M. Bodaghi, M. Tahriri, Ammonia-free method for synthesis of CdS nanocrystalline thin films through chemical bath deposition technique, Solid State Commun. 149 (2009) 1765–1768, https://doi.org/10.1016/j.ssc.2009.07.027.
[47] J.J. Ramsden, M. Grätzel, Photoluminescence of small cadmium sulphide particles, J. Chem. Soc., Faraday Trans. 80 (1984) 919–933, https://doi.org/10.1039/f19848000919.